Genetic Mapping of Monocyte Fate Decisions Following Myocardial Infarction

Authors:

Andrew L Koenig[1], Farid F Kadyrov[1], Junedh M Amrute[1], Steven Yang[1], Carla J Weinheimer[1], Jessica M Nigro[1], Attila Kovacs[1], Gabriella Smith[1], Kory J Lavine[1,2,3,#]

Affiliations:

[1]Center for Cardiovascular Research, Division of Cardiology, Department of Medicine, Washington University School of Medicine, Saint Louis, MO, 63110, USA.

[2]Department of Pathology and Immunology, Washington University School of Medicine, Saint Louis, MO, 63110, USA.

[3]Department of Developmental Biology, Washington University School of Medicine, Saint Louis, MO, 63110, USA.

[#]Correspondence should be addressed to:

Kory J. Lavine, MD, PhD,
Division of Cardiology, Department of Medicine, Washington University School of Medicine.
Address: 660 S Euclid, Campus Box 8086, St. Louis, MO 63110.
Telephone:314-362-1171
Email: klavine@wustl.edu

Abstract

Inflammation contributes to the pathogenesis of cardiac disease and represents a viable therapeutic target for heart failure. Cardiac injury elicits recruitment of neutrophils, monocytes, and T-cells. Monocytes and their progeny represent are highly abundant, display incredible functional diversity, and are key determinants of myocardial inflammation. Much remains to be learned regarding mechanisms and signaling events that instruct monocyte fate decisions. We devised a genetic lineage tracing strategy using *Ccr2*^{crERT2}*Rosa2*$^{LSL\text{-}tdTomato}$ mice in combination with single cell RNA-sequencing to map the fate and differentiation trajectories of monocytes that infiltrate the heart after reperfused myocardial infarction (MI). We observe that monocyte recruitment is restricted to the first 5 days following MI. Infiltrating monocytes give rise to transcriptionally distinct and spatially restricted macrophage and dendritic cell-like subsets, dynamically shift over time, and chronically persist within the myocardium. Pseudotime analysis predicted two differentiation trajectories of monocyte-derived macrophages that are initially partitioned into the border and infarct zones, respectively. Among these trajectories, we show that macrophages expressing a type I IFN responsive signature are an intermediate population localized within the border zone and promote myocardial protection. Collectively, these data uncover new complexities of monocyte differentiation in the infarcted heart and suggest that modulating monocyte fate decisions may have clinical implications.

Introduction

Myocardial infarction (MI) remains a leading cause of death and major cause of heart failure worldwide.[1,2] It is well established that ischemic damage to the heart promotes myocardial inflammation by triggering recruitment of peripheral leukocytes, acting as a second hit to the heart, leading to additional cardiomyocyte loss, fibrosis, adverse left ventricular (LV) remodeling, and impaired cardiac function. Among recruited leukocytes, monocytes and macrophages represent the most abundant immune cell to accumulate within the infarcted and failing heart.[3]

Within the past decade, it has been established that cardiac macrophages are functionally heterogeneous and can be broadly divided into two populations distinguished by expression of C-C chemokine receptor 2 (CCR2). $CCR2^-$ macrophages are an embryonically derived tissue resident population that comprise the major macrophage subset in the healthy heart. $CCR2^-$ macrophages are self-replenishing, express conserved markers of tissue resident macrophages, and function to orchestrate cardiac development, homeostasis, adaptation, and repair.[4–9] In contrast, $CCR2^+$ macrophages are an inflammatory population derived from recruited $LY6C^{hi}$ monocytes that accumulate within the injured and chronically failing heart. $CCR2^+$ macrophages are associated with and causally linked to heart failure as they contribute to damaging inflammation, myocardial fibrosis, and adverse LV remodeling.[6,10–17]

Recent studies from our group have leveraged single cell transcriptomics in both mice and humans to demonstrate additional complexity within cardiac monocyte and macrophage populations. [3,18–22] These studies have uncovered incredible diversity amongst $CCR2^+$ monocyte-derived macrophages that infiltrate the infarcted heart. While these findings have suggested that monocytes may differentiate into function diverse sub-populations of $CCR2^+$ macrophages, little is known regarding the spatial-temporal dynamics, trajectories, and mechanisms by which monocytes differentiate into these populations.

Results

Monocytes are recruited to the heart early after MI and their progeny chronically persist within the myocardium. To trace the fates of monocytes and their progeny after MI, we subjected *Ccr2*^{CreERT2}*Rosa26*$^{LSL\text{-}tdTomato}$ mice to closed-chest ischemia reperfusion injury to model reperfused MI.[23–25] *Ccr2*^{CreERT2} mice harbor a tamoxifen inducible CRE recombinase inserted into the 3' UTR of the *Ccr2* locus. We optimized a tamoxifen induction strategy to exclusively label circulating monocytes and not cardiac macrophages. A single injection of tamoxifen (60mg/kg, IP) into naïve mice achieved selective tdTomato labeling of Ly6c^{hi} monocytes in the blood at >80% efficiency 24 hours after injection. Cardiac macrophages did not express tdTomato (**Fig. 1A**). We also did not detect significantly tdTomato labeling of other major immune populations in the blood or their progenitors within the bone marrow compartment (**Suppl. Fig. 1**). As such, this strategy allows lineage tracing of infiltrating monocytes and their progeny independent of resident macrophages.

We then applied this labeling strategy to mice subjected to closed chest ischemia-reperfusion injury. Tamoxifen was injected 1 day prior to injury. Blood was collected from mice at days 1, 3, 5, 7, 13, and 28 after injury and hearts were collected at days 3, 7, 13, and 28 after injury (**Fig. 1B**). Flow cytometry analysis demonstrated >80% tdTomato labeling efficiency in Ly6c^{hi} monocytes in the blood 1 day post-MI. The percent of Ly6c^{hi} monocytes labeled progressively decreased throughout the first 7 days post-MI and was absent thereafter. Intriguingly, the progeny of monocytes that entered the heart during this labeling window remained present for at least 28 days post-MI. Continuous labeling of monocytes by tamoxifen injection (60mg/kg IP, every 3 days) did not demonstrate additional labeling of cardiac macrophages (**Fig. 1C**). Labeling of macrophages within the heart was validated at each time point by visualization of tdTomato and immunostaining for CD68 (**Fig. 1D-E**). These findings indicate that monocytes enter the heart predominately within 5-7 days post-MI and their progeny including monocyte-derived macrophages persist within the myocardium for at least 28 days post-MI.

Macrophage states dynamically shift over time after injury. To delineate the temporal dynamics of recruited monocytes and their progeny, we performed single cell RNA-sequencing of monocytes and macrophages sorted from *Ccr2*^{CreERT2}*Rosa26*$^{LSL\text{-}tdTomato}$ hearts collected at days 3, 7, 13, and 28 post-MI (**Fig. 1B, Suppl. Fig. 2A**). Libraries were constructed for each time point, sequenced, aligned using Cellranger, and then integrated, clustered, and analyzed using Seurat.[26,27] We identified 10 transcriptionally distinct cell clusters: monocytes, dendritic cells, and 8 macrophage states (**Fig. 2A**). We performed differential expression analysis and constructed z-score signatures to validate that the observed clusters were transcriptionally distinct (**Fig. B-C, Suppl. Fig. 3**). When cells were compared across time points, it was evident that macrophage states significantly shifted over time. At 3 day post-MI, the predominant populations within the heart consisted of monocytes, proliferating macrophages, *Arg1*$^{+}$ macrophages, type-1 interferon activated macrophages, and *Trem2*$^{+}$ macrophages. Through days 7 and 13 post-MI we observed decreases in frequency of monocytes, proliferating cells, *Arg1*$^{+}$ macrophages, and type-1 interferon activated macrophages. *Trem2*$^{+}$ macrophages and *Gdf15*$^{+}$ macrophages expanded during this time interval. By day 28 post MI, macrophages had transitioned to a predominantly MHCII^{hi} state (**Fig. 2D-E**).

We additionally performed custom alignment of the libraries to the tdTomato coding sequence and observed that all identified clusters were labeled by expression of tdTomato. Interestingly, a proportion of macrophages within the resident cluster were also labeled by tdTomato indicating

that recruited macrophages have the potential to adopt a resident-like fate. (**Fig. 2F, Suppl. Fig. 3**). We next examined the dynamics of tdTomato$^+$ cells as a function of time and found that tdTomato$^+$ cells were substantially distributed across cell states at day 3 post-MI. At day 7 post-MI number of tdTomato$^+$ monocytes, *Arg1*$^+$ macrophages, type-1 interferon activated macrophages, and proliferating macrophages declined and a shifts towards *Gdf15*$^+$ and *Trem2*$^+$ macrophages was evident. At day post-MI the majority of tdTomato$^+$ cells were MHCII^{hi} macrophages (**Fig. 2G**). Together, these results demonstrate that monocyte recruitment occurs within the first week after MI, their progeny persist within the heart at chronic stages after MI, and that monocytes display incredible plasticity differentiating into multiple transcriptionally distinct subsets that dynamically shift over time.

Resident macrophages do not contribute to states observed in recruited macrophages. We utilized *Cx3cr1*^{CreERT2}*Rosa26*$^{LSL\text{-}tdTomato}$ mice to evaluate the contribution of resident macrophages to the diverse subsets of monocyte-derived macrophages that emerge following MI. Utilizing a pulse-chase strategy, we injected mice with tamoxifen (60mg/kg daily X5 days) 2 weeks prior to ischemia reperfusion injury (**Fig. 3A**). This strategy specifically labels long-lived resident macrophages with tdTomato. Monocytes are not labeled as they are replenished by unlabeled monocytes during the chase period.[13] Macrophage and monocytes were sorted via FACS into tdTomato$^+$ (resident) and tdTomato$^-$ (recruited) libraries for single cell RNA sequencing (**Fig. 3A, Suppl. Fig. 2B**). We observed that resident macrophages clustered independently of recruited macrophages and displayed distinct transcriptional profiles. Moreover, genes representative of monocyte-derived macrophage states were enriched in the recruited library, while classical markers of cardiac resident macrophages were specifically present with the resident library (**Fig. 3B-C**). To validate that the labeling of these populations was efficient, we again aligned the single cell libraries to the tdTomato coding sequence and found that tdTomato was exclusively expressed in cells found within the resident macrophage library (**Fig. 3D-E**). These data indicate that resident macrophages do not contribute to the diverse macrophage subsets marked by *Ccr2-CreERT2* lineage tracing, consistent with their origin from infiltrating monocytes.

***Arg1*-expression and interferon activated macrophages are predicted as early transient macrophage states.** To assess whether these diverse macrophage populations exist in different regions of the heart, we utilized a published spatial transcriptomic dataset of mouse MI.[28] We plotted z-scores of the individual macrophage states onto transverse heart sections at 7 days post-MI and observed that individual monocyte, cDC, and macrophage states are enriched in different regions of the infarct. Arg1$^+$, Trem2$^+$, Gdf15$^+$, and Ccl8$^+$ macrophages are enriched near the core of the infarct. Type-1 interferon activated macrophages, cDC2s and monocytes are enriched in the border zone. MHCII^{hi} macrophages localized to the infarct and border zones. Resident macrophage are predominantly found outside of the infarct in the remote zone of the heart, while proliferating macrophages are distributed within the infarct and remote zones (**Fig. 4A**).

We also utilized Palantir to perform pseudotime lineage tracing analysis.[29] We presented the data using force directed layout (FDL) projections split by cell state and time point post-MI (**Fig. 4B-C**). We selected monocytes from the day 3 post-MI dataset as the starting cell. Palantir predicted that cDC2s, Trem2$^+$ macrophages, and MHCII^{hi} macrophages were terminal cell states and that type-1 interferon activated macrophages and Arg1$^+$ macrophages represented intermediate states of differentiation based on entropy and pseudotime scores. Consistent with this frame work, monocytes, Arg1$^+$ macrophages, and type-1 interferon activated macrophages were enriches at early time points post-MI (**Fig. 4C-D**) and positioned directly adjacent to monocytes in pseudotime vs. entropy waterfall plots (**Fig. 4E).** Taken together, these data

predict that monocytes differentiate into spatially restricted macrophage subsets and that type-1 interferon activated macrophages and Arg1^{+} macrophages represent distinct intermediate macrophage populations.

Type I interferon signaling in monocytes and monocyte-derived macrophages protects from adverse post-MI remodeling. To gain initial insights into the function diversity of monocyte-derived macrophages, we chose to focus on the type I IFN activated macrophage subset. We generated *Ccr2*^{CreERT2}*Ifnar1*^{Flox} mice to selectively delete *Ifnar1* in recruited monocytes and their progeny (**Fig. 5A**).[30] Control and *Ccr2*^{CreERT2}*Ifnar1*^{Flox} mice were subjected to MI and echocardiography performed at day 28 post injury. Mice were either treated with a single dose of tamoxifen (60mg/kg IP) 1 day prior to MI or continuous tamoxifen dosing to target monocytes that enter the heart within the first week or all infiltrating monocytes, respectively. *Ccr2*^{CreERT2}*Ifnar1*^{Flox} hearts demonstrated significantly increased end systolic and diastolic left ventricular volumes and increased akinetic area compared to controls (**Fig. 5B-C**). Analysis of cardiomyocyte size via wheat-germ agglutinin staining revealed increased cardiomyocyte hypertrophy in the border and remote zones of the left ventricle along with increased infarct size as measured with trichrome staining in *Ccr2*^{CreERT2}*Ifnar1*^{Flox} hearts relative to controls (**Fig. 5D-F**). These findings were evident between tamoxifen dosing strategies, consistent with the concept that type I interferon signaling in monocytes and monocyte-derived macrophages occurs early after MI (**Fig 5C-E**). These findings indicate that type I interferon signaling plays a temporal and cell type specific protective role in post-MI remodeling.[31]

Discussion

In summary, our data provides new insights into the spatiotemporal dynamics of monocyte recruitment and differentiation following MI. Monocytes are recruited into the myocardium within the first 5-7 days post-MI and their progeny persisted through at least 28 days post-MI. Single cell RNA sequencing combined with genetic lineage tracing provided an unprecedented opportunity to precisely define the fates of monocytes that infiltrate the infarcted heart. This technique enabled the identification of monocyte, macrophage, and cDC2 populations that reside within the infarcted heart and demonstrated a coordinated and dynamic shift in macrophage phenotype over time. Furthermore, we demonstrated that these diverse macrophage subsets are situated in distinct locations within the heart and that type-1 interferon activated macrophages and Arg1^{+} macrophages are predicted as intermediate populations that give rise to more terminal macrophage states. Within this framework, type I interferon activated macrophages confer protection following MI by reducing adverse LV remodeling and infarct expansion. These findings uncover the complexity of monocyte fate decisions and highlight the therapeutic potential for targeting monocyte differentiation.

Methods

Animal Models. Mus musculus were housed in ultraclean rodent barrier facility with veterinarians from the Washington University Division of Comparative Medicine on call or on site for animal care. All procedures were performed in accordance with IUCAC protocols. Strains used were *Cx3cr1*^{ERT2Cre} [32] (JAX #020940), (JAX #007561), *Rosa26*$^{lox\text{-}stop\text{-}lox\ tdTomato}$ [33] (JAX #007914), *CCR2*^{ERT2Cre} [34], and *Ifnar1*^{Flox} [30] (JAX # 028256) on the C57BL/6 background. Experiments were performed on mice 6-12 weeks of age. Equal numbers of male and female mice were used for experiments. For Cre recombination in all monocytes and macrophages, *Ccr2*^{CreERT2} *Ifnar1*$^{flox/flox}$ mice were given tamoxifen food pellets (Envigo TD.130857) for the entirety of the experiment. For Cre recombination in other lines, mice were given IP injection of 60 mg/kg of tamoxifen (Millipore Sigma T5648) at the indicated frequency and timing.

Closed-chest Ischemia Reperfusion Injury. Mice were anesthetized, intubated, and mechanically ventilated. The heart was exposed, and a suture placed around the proximal left coronary artery. The suture was threaded through a 1 mm piece of polyethylene tubing to serve as the arterial occlude. Each end of the suture was exteriorized through the thorax. The skin was closed, and mice were given a 2-week recovery period prior to induction of ischemia. After 2 weeks, the animals were anesthetized and placed on an Indus Mouse Surgical Monitor system to accurately record ECG during ischemia. Ischemia was induced after anesthetizing the animals. Tension was exerted on suture ends until ST-segment elevation was seen via ECG. Following 90 minutes of ischemia time, tension was released, and the skin was then closed.

Echocardiography. Mice were sedated with Avertin (0.005 ml/g) and 2D and M-mode images were obtained in the long and short axis views 4 weeks after MI using the VisualSonics770 Echocardiography System. Left diastolic volume, left systolic volume, akinetic area, and total LV area was measured using edge detection and tracking software (VivoLab). Ejection fraction was calculated as the (left diastolic volume – left systolic volume) / left diastolic volume. Akinetic percentage was calculated as the akinetic area / total LV area.

Histology. 4 weeks after MI, mice were euthanized, and hearts perfused with PBS. Hearts were fixed overnight with 4% PFA in PBS at 4□C, cut into thirds on the transverse plane, placed into histology cassettes for paraffin embedding, and dehydrated in 70% ethanol in water. Hearts were paraffin embedded and cut into 4 µm sections and mounted on positively charged slides. Tissues were stained by Gomori's Trichrome staining (Richard-Allan Scientific 87020) and WGA staining (Vector Laboratories RL-1022). Trichrome staining was imaged using a Meyer PathScan Enabler IV. Measurement of infarct length and LV length was performed in FIJI, with data quantification normalizing the length of the infarct to the length of the LV[35]. WGA staining was imaged using the 20x objective of a Zeiss Axioscan7 confocal microscope. 3 20x fields of the border zone of the infarct were randomly selected per mouse. 20 cross sectional (not longitudinal) cardiomyocytes per 20x field were selected at random. Measurement of cross-sectional cardiomyocyte area was performed in FIJI. Data is displayed as the average cardiomyocyte cross sectional area per mouse.

Immunofluorescence. Mice were euthanized, and hearts perfused with PBS. Hearts were cut midway on the transverse plane and fixed overnight with 4% PFA in PBS at 4□C. They were then dehydrated in 30% sucrose in PBS overnight at 4□C. Hearts were embedded in O.C.T.

(Sakura 4583) and frozen at -80□C for 30 minutes. Hearts were then sectioned at 15 µm using a Leica Cryostat, mounted on positively charged slides, and stored at -80□C. For staining, the following steps were performed at room temperature and protected from light. Slides were brought to room temperature for 5 minutes and washed in PBS for 5 minutes. Sections were then permeabilized in 0.25% Triton X in PBS for 5 minutes. Sections were then blocked in 5% BSA in PBS for 1 hour. Sections were then stained with primary antibody diluted in 1% BSA in PBS for 1 hour with rat anti CD68 (BioLegend 137002 1:400 dilution), rabbit anti Lyve1 (abcam ab14917 1:200 dilution). Sections were then washed 3 times 5 minutes each with PBS-Tween. After washing, the appropriate secondary antibodies were added diluted in 1% BSA in PBS for 1 hour at a 1:1000 dilution (Goat anti Rat 488 Life Technologies a11006, Donkey anti Rabbit 647 Abcam ab150075,). Slides were again washed 3 times 5 minutes each with PBS-T, and then mounted with DAPI mounting media (Millipore Sigma F6057) and cover slipped. Slides were stored at 4□C protected from light and imaged within 1 week.

Slides were imaged using the 20x objective of a Zeiss Axioscan7 microscope. Visualization of tdTomato was from the endogenous signal. For quantification, 3-5 20x fields were randomly selected per mouse of either the remote zone or infarct zone as indicated. Quantification of cell numbers were performed in FIJI or Zeiss Zen, and data is displayed as the average of each 20x field per mouse.

Flow Cytometry. Hearts were perfused with PBS, weighed, minced, and digested for 45 minutes at 37□C in DMEM (Gibco 11965-084) containing 4500 U/ml Collagenase IV (Millipore Sigma C5138), 2400 U/ml Hyaluronidase I (Millipore Sigma H3506), and 6000 U/ml DNAse I (Millipore Sigma D4527). Enzymes were deactivated with HBSS containing 2% FBS and 0.2% BSA and filtered through 40-micron strainers. Cells were incubated with ACK lysis buffer (Gibco A10492-01) for 5 minutes at room temperature. Cells were washed with DMEM and resuspended in 100 µl of FACS buffer (PBS containing 2% FBS and 2mM EDTA).

Approximately 100 µl of blood was collected by cheek bleed into a tube containing 20 µl of EDTA (Corning 46-034-CI). Cells were incubated with ACK lysis buffer for 15 minutes at room temperature, washed, and ACK lysed a second time. Cells were then washed with DMEM and resuspended in 100 µl of FACS buffer.

Cells were incubated in a 1:200 dilution of fluorescence conjugated monoclonal antibodies for 30 minutes at 4□C. Samples were washed in FACS buffer and resuspended in a final volume of 250 µl FACS buffer. Flow cytometry and sorting was performed using a BD FACS melody.

For sorting of monocytes and macrophages from *Cx3cr1*^{CreERT2}*Rosa26*$^{LSL\text{-}tdTomato}$ for single cell RNA sequencing, antibodies used were: CD45 PerCP/Cy5.5 (BioLegend 103132), Ly6g APC/Cy7 (BioLegend 127623), Ly6c APC (BioLegend 128016), CD64 PE/Cy7 (BioLegend 139313), and Cd11b BV421 (BioLegend 101235).

For sorting of monocytes and macrophages from *Ccr2*^{CreERT2}*Rosa26*$^{LSL\text{-}tdTomato}$ for single cell RNA sequencing, antibodies used were: CD45 PerCP/Cy5.5 (BioLegend 103132), Ly6g APC/Cy7 (BioLegend 127623), Ly6c FITC (BioLegend 128005), and CD64 APC (BioLegend 164409), Cd11b PE/Cy7 (BioLegend 101215), CD3 BV510 (BioLegend 100233), CD19 BV510 (BioLegend 115545) and MHCII BV421 (BioLegend 107631).

For flow cytometry of blood from *Ccr2*^{CreERT2}*Rosa26*$^{LSL\text{-}tdTomato}$, antibodies used were: CD45 PerCP/Cy5.5 (BioLegend 103132), Ly6g BV421 (BioLegend 127627), Ly6c PE/Cy7 (BioLegend 128017), CD115 APC (BioLegend 135509), CD3 FITC (BioLegend 152303), and CD19 BV510 (BioLegend 115545) .

For flow cytometry of bone marrow from *Ccr2*^{CreERT2}*Rosa26*$^{LSL\text{-}tdTomato}$, antibodies used were: Sca1 FITC (BioLegend 108105), c-Kit PerCP/Cy5.5 (BioLegend 135133), Il7ra PE/Cy7

(BioLegend 158209), CD34 APC (BioLegend 119309), CD16/CD32 APC/Cy7 (BioLegend 156611), and Lineage Cocktail BV421 (BioLegend 133311).

Single Cell RNA Sequencing Analysis. Monocytes and macrophages were sorted after I/R as indicated. Single cell RNA sequencing libraries were generated using the 10X Genomics 5'v1 platform. Libraries were sequenced using a NovaSeq 6000 at the McDonnel Genome Institute (MGI). For *Cx3cr1*^{CreERT2}*Rosa26*$^{LSL\text{-}tdTomato}$ mice, cells were separated into tomato- and tomato+ libraries. Sequencing reads were aligned to the GRcm38 transcriptome using CellRanger (v3.1.0) from 10X Genomics. Custom

Downstream data processing was performed in the R package Seurat (v4)[36]. SCtransform was used to scale and normalize the data for RNA counts. Quality control filters of genes/cell>200, mitochondrial reads/cell<10%, read counts/cell>5000, and read counts/cell<40000 were applied. PCA was used for dimensionality reduction, data was clustered at multiple resolutions, and UMAP projections were generated for data visualization. Harmony integration was applied to account for batch effect from different time points[37]. Contaminating populations of neutrophils and non-myeloid cells were excluded from analysis. Differential gene expression of upregulated genes in each subpopulation was generated in Seurat using FindAllMarkers with a minimum fraction (min.pct) of 0.1 and a logFC threshold of 0.1. Differential gene expression between macHif1aKO and control mice was performed through Seurat using DEseq2[38]. Gaussian kernel density estimation plots were generated using the Python package Scanpy (v1.8.1)[39].

Palantir Trajectory Analysis. The Palantir Python package was used for trajectory analysis (v1.0.0 to v1.1)[29]. Prior to inputting data to Palantir, cell cycle regression was performed using Seurat. Monocytes were used as the early and starting cell type for Palantir. Highly variable gene analysis was not used. The eigenvectors used was determined by the eigengap. The number of waypoints used was 500. The option to use the early cell as the start cell was used. The output pseudotime/entropy values, terminal state probabilities, and FDL coordinates for each cell was used to generate plots in R.

Spatial transcriptomics. Spatial transcriptomics data of Arg1 macrophage localization was generated using a published data set of mouse MI 7 days after injury (GSE176092)[28]. Spatial data was analyzed using Seurat. The macrophage population gene signature was plotted by calculating the Z-score of the genes as listed and using the function "SpatialFeaturePlot" using the Z-score as a feature.

Statistical Analysis For analysis of echocardiography, histology, and immunofluorescence, two tailed t-test assuming equal variance was performed in GraphPad Prism. At least 3 replicates were used for experiments. $P < 0.05$ was a priori considered statistically significant. Data was plotted using Prism software.

Data Availability

Single Cell RNA sequencing data will be available on the Gene Expression Omnibus at the time of publication.

Code Availability

R and Python scripts are available on GitHub (https://github.com/alkoenig/Cardiac_Monocyte_Fate).

References Cited

1. Lesyuk, W., Kriza, C. & Kolominsky-Rabas, P. Cost-of-illness studies in heart failure: a systematic review 2004-2016. *BMC Cardiovasc Disord* **18**, 74 (2018).

2. Ziaeian, B. & Fonarow, G. C. Epidemiology and aetiology of heart failure. *Nat Rev Cardiol* **13**, 368–378 (2016).

3. Koenig, A. L. *et al.* Single-cell transcriptomics reveals cell-type-specific diversification in human heart failure. *Nat Cardiovasc Res* **1**, 263–280 (2022).

4. Leid, J. *et al.* Primitive Embryonic Macrophages are Required for Coronary Development and Maturation. *Circ Res* **118**, 1498–1511 (2016).

5. Wong, N. R. *et al.* Resident cardiac macrophages mediate adaptive myocardial remodeling. *Immunity* **54**, 2072-2088.e7 (2021).

6. Lavine, K. J. *et al.* Distinct macrophage lineages contribute to disparate patterns of cardiac recovery and remodeling in the neonatal and adult heart. *Proc Natl Acad Sci U S A* **111**, 16029–16034 (2014).

7. Wang, Y. *et al.* Mitochondrial Fission Promotes the Continued Clearance of Apoptotic Cells by Macrophages. *Cell* **171**, 331-345.e22 (2017).

8. Hulsmans, M. *et al.* Macrophages Facilitate Electrical Conduction in the Heart. *Cell* **169**, 510-522.e20 (2017).

9. Dick, S. A. *et al.* Three tissue resident macrophage subsets coexist across organs with conserved origins and life cycles. *Science Immunology* **7**, eabf7777 (2022).

10. Bajpai, G. *et al.* The human heart contains distinct macrophage subsets with divergent origins and functions. *Nat Med* **24**, 1234–1245 (2018).

11. Lavine, K. J. *et al.* The Macrophage in Cardiac Homeostasis and Disease: JACC Macrophage in CVD Series (Part 4). *J Am Coll Cardiol* **72**, 2213–2230 (2018).

12. Li, W. *et al.* Heart-resident CCR2+ macrophages promote neutrophil extravasation through TLR9/MyD88/CXCL5 signaling. *JCI Insight* **1**, 87315 (2016).

13. Bajpai, G. *et al.* Tissue Resident CCR2- and CCR2+ Cardiac Macrophages Differentially Orchestrate Monocyte Recruitment and Fate Specification Following Myocardial Injury. *Circ Res* **124**, 263–278 (2019).

14. Feng, G. *et al.* CCL17 Aggravates Myocardial Injury by Suppressing Recruitment of Regulatory T Cells. *Circulation* **145**, 765–782 (2022).

15. van Amerongen, M. J., Harmsen, M. C., van Rooijen, N., Petersen, A. H. & van Luyn, M. J. A. Macrophage Depletion Impairs Wound Healing and Increases Left Ventricular Remodeling after Myocardial Injury in Mice. *Am J Pathol* **170**, 818–829 (2007).

16. Majmudar, M. D. *et al.* Monocyte-Directed RNAi Targeting CCR2 Improves Infarct Healing in Atherosclerosis-Prone Mice. *Circulation* **127**, 2038–2046 (2013).

17. Patel, B. *et al.* CCR2+ Monocyte-Derived Infiltrating Macrophages Are Required for Adverse Cardiac Remodeling During Pressure Overload. *JACC: Basic to Translational Science* **3**, 230–244 (2018).

18. Litviňuková, M. *et al.* Cells of the adult human heart. *Nature* **588**, 466–472 (2020).

19. Tucker, N. R. *et al.* Transcriptional and Cellular Diversity of the Human Heart. *Circulation* **142**, 466–482 (2020).

20. Liu, J. *et al.* Transcriptional and Immune Landscape of Cardiac Sarcoidosis. *Circ Res* **131**, 654–669 (2022).

21. Wang, L. *et al.* Single-cell reconstruction of the adult human heart during heart failure and recovery reveals the cellular landscape underlying cardiac function. *Nat Cell Biol* **22**, 108–119 (2020).

22. Nicin, L. *et al.* Single Nuclei Sequencing Reveals Novel Insights Into the Regulation of Cellular Signatures in Children With Dilated Cardiomyopathy. *Circulation* **143**, 1704–1719 (2021).

23. Chen, H.-R. *et al.* Fate mapping via CCR2-CreER mice reveals monocyte-to-microglia transition in development and neonatal stroke. *Science Advances* **6**, eabb2119.

24. Madisen, L. *et al.* A robust and high-throughput Cre reporting and characterization system for the whole mouse brain. *Nat Neurosci* **13**, 133–140 (2010).

25. Snippert, H. J. *et al.* Intestinal Crypt Homeostasis Results from Neutral Competition between Symmetrically Dividing Lgr5 Stem Cells. *Cell* **143**, 134–144 (2010).

26. Hao, Y. *et al.* Integrated analysis of multimodal single-cell data. *bioRxiv* 2020.10.12.335331 (2020) doi:10.1101/2020.10.12.335331.

27. Stuart, T. *et al.* Comprehensive Integration of Single-Cell Data. *Cell* **177**, 1888-1902.e21 (2019).

28. Yamada, S. *et al.* Spatiotemporal transcriptome analysis reveals critical roles for mechano-sensing genes at the border zone in remodeling after myocardial infarction. *Nat Cardiovasc Res* **1**, 1072–1083 (2022).

29. Setty, M. *et al.* Characterization of cell fate probabilities in single-cell data with Palantir. *Nat Biotechnol* **37**, 451–460 (2019).

30. Kamphuis, E., Junt, T., Waibler, Z., Forster, R. & Kalinke, U. Type I interferons directly regulate lymphocyte recirculation and cause transient blood lymphopenia. *Blood* **108**, 3253–3261 (2006).

31. King, K. R. *et al.* IRF3 and Type I Interferons Fuel a Fatal Response to Myocardial Infarction. *Nat Med* **23**, 1481–1487 (2017).

32. Yona, S. *et al.* Fate Mapping Reveals Origins and Dynamics of Monocytes and Tissue Macrophages under Homeostasis. *Immunity* **38**, 79–91 (2013).

33. Madisen, L. *et al.* A robust and high-throughput Cre reporting and characterization system for the whole mouse brain. *Nat Neurosci* **13**, 133–140 (2010).

34. Croxford, A. L. *et al.* The Cytokine GM-CSF Drives the Inflammatory Signature of CCR2+ Monocytes and Licenses Autoimmunity. *Immunity* **43**, 502–514 (2015).

35. Schindelin, J. *et al.* Fiji: an open-source platform for biological-image analysis. *Nat Methods* **9**, 676–682 (2012).

36. Hao, Y. *et al.* Integrated analysis of multimodal single-cell data. *Cell* **184**, 3573-3587.e29 (2021).

37. Korsunsky, I. *et al.* Fast, sensitive, and accurate integration of single cell data with Harmony. 461954 Preprint at https://doi.org/10.1101/461954 (2018).

38. Love, M. I., Huber, W. & Anders, S. Moderated estimation of fold change and dispersion for RNA-seq data with DESeq2. *Genome Biology* **15**, 550 (2014).

39. Wolf, F. A., Angerer, P. & Theis, F. J. SCANPY: large-scale single-cell gene expression data analysis. *Genome Biol* **19**, 15 (2018).

Figure Legends

Fig. 1 Recruited monocyte-derived macrophages persist in the heart after myocardial infraction

Schematic of tamoxifen dosing strategy for tdTomato labeling of recruited monocyte and macrophages. Representative flow cytometry plots demonstrate high labeling efficiency in monocytes in the blood, while resident macrophages remain predominantly unlabeled (A). Diagram of experimental strategy for monocyte labeling time course (B). Bar graphs demonstrating tdTomato labeling of blood monocytes (left) and heart tissue monocyte and macrophages (right, single inj: single dose labeling, cont: continuous labeling) (C). Quantification of tdTomato+ macrophages out of total CD68 positive macrophages by IHC (D). Representative images of IHC (E).

Fig. 2 Recruited macrophage populations shift transcriptionally over time after myocardial infarction

Clustered UMAP projection of combined single cell libraries from all 4 time points (A). UMAP plots of calculated z-scores for each cluster (B, list of genes in z-score below). Dot plot of z-scores by cluster (C). UMAP projection of single cell libraries split by time point after injury (left) and proportion of cells in each cluster split by time point (right) (D). UMAP plots of density by time after injury (E). UMAP plot of combined time points labeled by tdTomato expression (F). Line graph of proportion of tdTomato+ cells in each cluster across time points (G).

Fig. 3 Resident macrophages do not contribute to the diverse populations of monocyte-derived macrophages.

Schematic of the experimental strategy for resident macrophage labeling (left) and FACS gating strategy for selecting tdTomato+ (resident) and tdTomato- (recruited) libraries (A). Combined UMAP plot of resident and recruited libraries labeled by library (B). Heatmap of enriched genes in each library from differential expression analysis (C). UMAP plot of tdTomato expression split by library (D). Violin plot of tdTomato expression split by library (E).

Fig. 4 Recruited macrophage populations are spatially and temporally distinct

Spatial transcriptomic expression plots of z-scores enriched in each identified cluster at day 7 post-MI (A). FDL projection of combined time points split by cluster (B) and time point (C). FDL projection labeled by pseudotime and differentiation potential (D). Pseudotime/Entropy waterfall plots colored by cluster (E).

Fig. 5 Type 1 interferon is protective against adverse remodeling

Experimental strategy for deleting *Ifnar* in recruited monocyte-derived macrophages (A). Representative echocardiographic images of end diastole (B). Quantification of echocardiography measurements (C). Measurement of cardiomyocyte size by WGA staining (D). Measurements of infarct size as percentage of LV diameter by trichrome staining (E). Representative images of WGA and trichrome staining (F). * $p<0.05$, *** $p<0.001$

Suppl. Fig. 1 Bone marrow and blood gating

Representative gates and quantification of percent tdTomato positive cells of indicated cell type by flow cytometry in naïve *Ccr2*^{CreERT2}*Rosa26*$^{LSL\text{-}tdTomato}$ mouse 1 day post tamoxifen injection in bone marrow (A, CLP: common lymphoid progenitor, CMP: common myeloid progenitor, GMP: granulocyte-monocyte progenitor, MEP: megakaryocyte-erythrocyte progenitor) and blood (B)

Suppl. Fig. 2 Single cell FACs gating strategies

Outline of gating strategies used for sorting cells for single cell RNA sequencing libraries for recruited macrophage time course (A) and resident labeling (B).

Suppl. Fig. 3 Z-scores of recruited macrophage labeling time course

Heatmap of top 5 enriched genes in each cluster from differential gene expression (A). UMAP projections of z-scores enriched in each cluster, split by time post injury (B). Example image demonstrating expression of Lyve1 resident macrophage marker in tdTomato+ recruited macrophage in *Ccr2*^{CreERT2}*Rosa26*$^{lsl\text{-}tdTomato}$ at day 28 post MI (C).

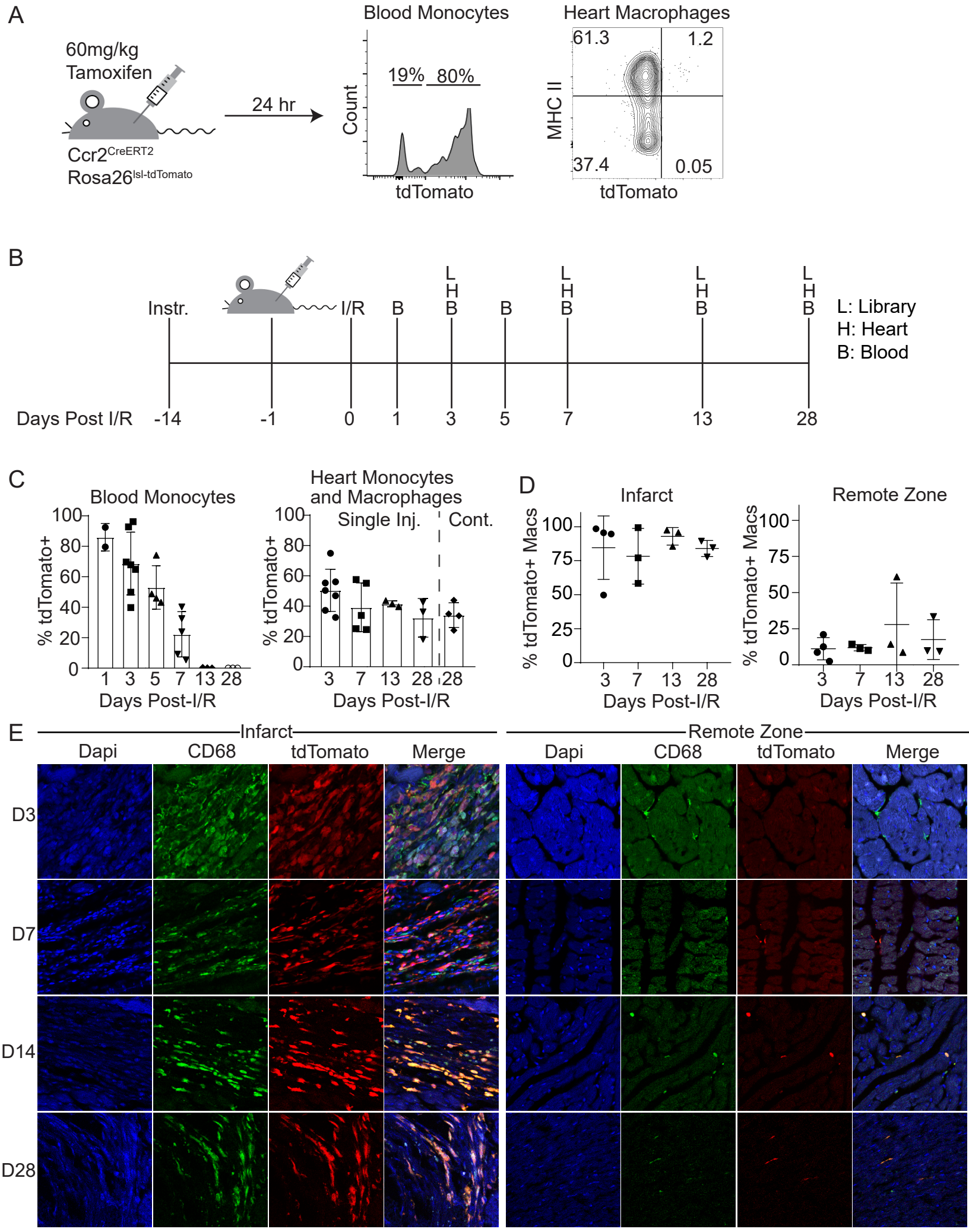
A
60mg/kg
Tamoxifen
Ccr2CreERT2
Rosa26lsl-tdTomato
24 hr
Blood Monocytes
19%
80%
Count
tdTomato
Heart Macrophages
61.3
1.2
37.4
0.05
MHC II
tdTomato
B
Instr.
I/R
B
L
H
B
B
L
H
B
L
H
B
L
H
B
L: Library
H: Heart
B: Blood
Days Post I/R
-14
-1
0
1
3
5
7
13
28
C
Blood Monocytes
% tdTomato+
Days Post-I/R
Heart Monocytes
and Macrophages
Single Inj.
Cont.
% tdTomato+
Days Post-I/R
D
Infarct
% tdTomato+ Macs
Days Post-I/R
Remote Zone
% tdTomato+ Macs
Days Post-I/R
E
Infarct
Remote Zone
Dapi
CD68
tdTomato
Merge
D3
D7
D14
D28

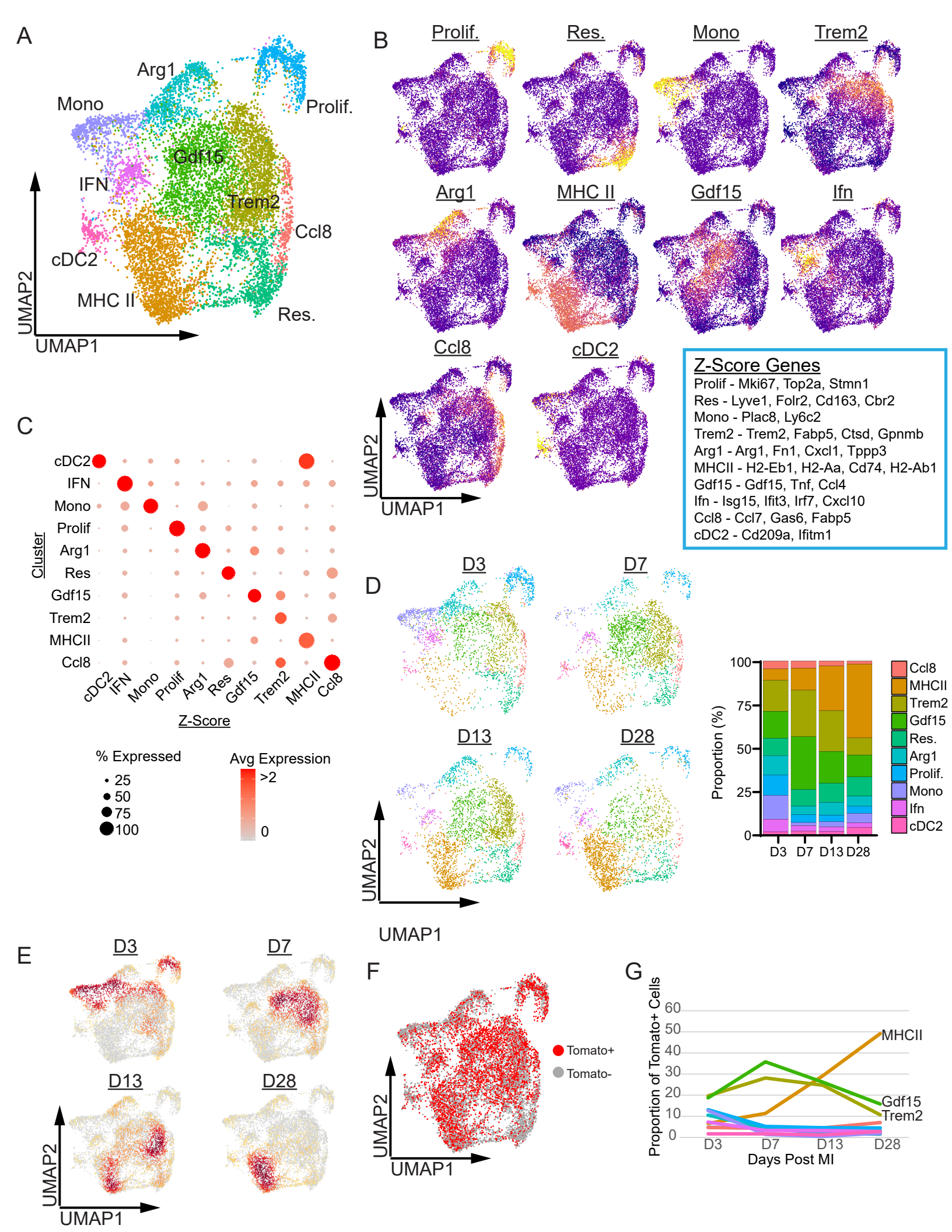
A
Arg1
Mono
Prolif.
Gdf15
IFN
Trem2
Ccl8
cDC2
MHC II
Res.
UMAP2
UMAP1
B
Prolif.
Res.
Mono
Trem2
Arg1
MHC II
Gdf15
Ifn
Ccl8
cDC2
UMAP2
UMAP1
Z-Score Genes
Prolif - Mki67, Top2a, Stmn1
Res - Lyve1, Folr2, Cd163, Cbr2
Mono - Plac8, Ly6c2
Trem2 - Trem2, Fabp5, Ctsd, Gpnmb
Arg1 - Arg1, Fn1, Cxcl1, Tppp3
MHCII - H2-Eb1, H2-Aa, Cd74, H2-Ab1
Gdf15 - Gdf15, Tnf, Ccl4
Ifn - Isg15, Ifit3, Irf7, Cxcl10
Ccl8 - Ccl7, Gas6, Fabp5
cDC2 - Cd209a, Ifitm1
C
cDC2
IFN
Mono
Prolif
Arg1
Res
Gdf15
Trem2
MHCII
Ccl8
Cluster
Z-Score
% Expressed
25
50
75
100
Avg Expression
>2
0
D
D3
D7
D13
D28
UMAP2
UMAP1
Proportion (%)
100
75
50
25
0
D3
D7
D13
D28
Ccl8
MHCII
Trem2
Gdf15
Res.
Arg1
Prolif.
Mono
Ifn
cDC2
E
D3
D7
D13
D28
UMAP2
UMAP1
F
Tomato+
Tomato-
UMAP2
UMAP1
G
Proportion of Tomato+ Cells
60
50
40
30
20
10
0
MHCII
Gdf15
Trem2
D3
D7
D13
D28
Days Post MI

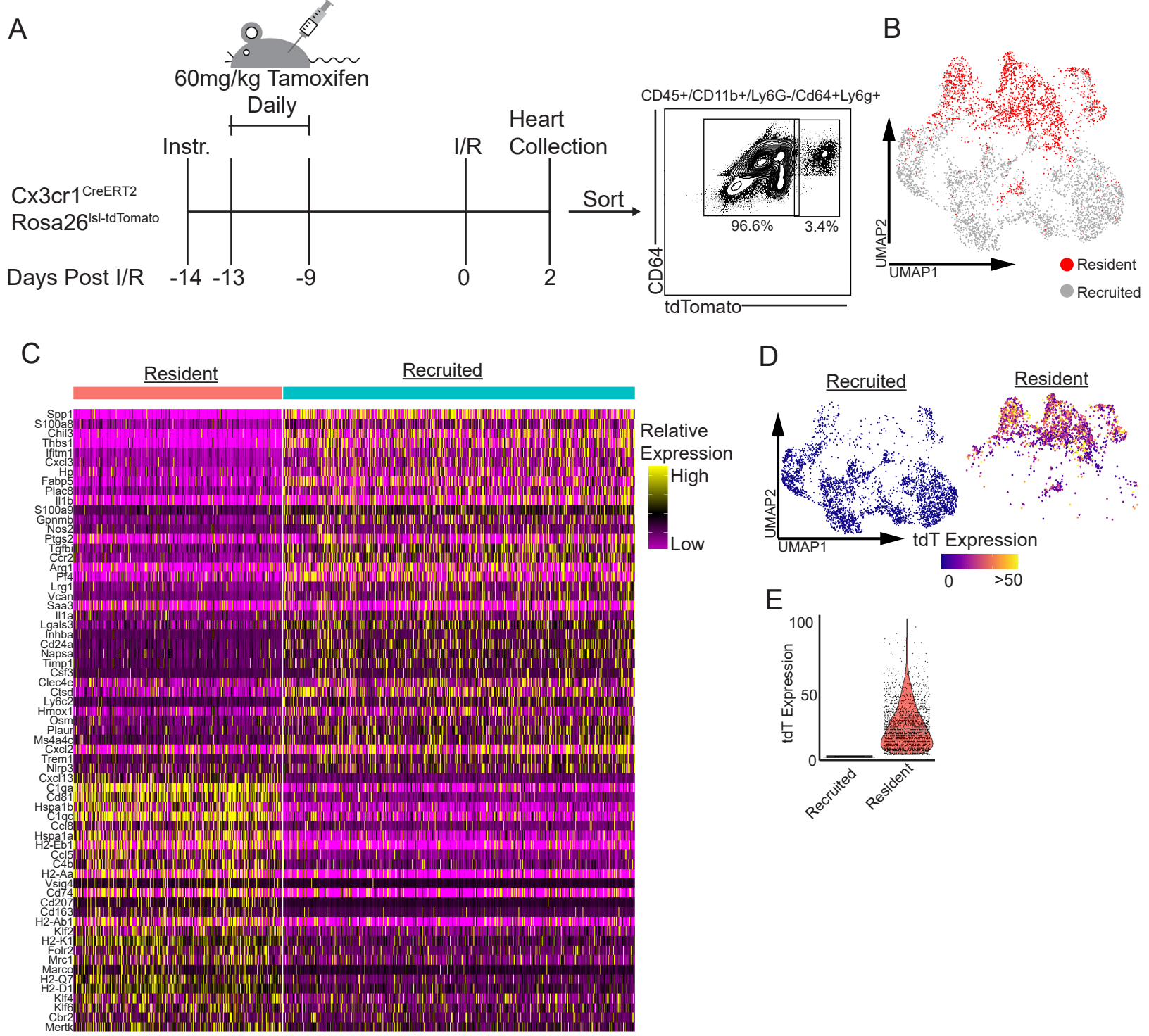
A
60mg/kg Tamoxifen
Daily
Instr.
I/R
Heart
Collection
Cx3cr1CreERT2
Rosa26lsl-tdTomato
Days Post I/R
-14
-13
-9
0
2
Sort
CD45+/CD11b+/Ly6G-/Cd64+Ly6g+
96.6%
3.4%
CD64
tdTomato
B
UMAP2
UMAP1
Resident
Recruited
C
Resident
Recruited
Relative
Expression
High
Low
Spp1
S100a8
Chil3
Thbs1
Ifitm1
Cxcl3
Hp
Fabp5
Plac8
Il1b
S100a9
Gpnmb
Nos2
Ptgs2
Tgfbi
Ccr2
Arg1
Pf4
Lrg1
Vcan
Saa3
Il1a
Lgals3
Inhba
Cd24a
Napsa
Timp1
Csf3
Clec4e
Ctsd
Ly6c2
Hmox1
Osm
Plaur
Ms4a4c
Cxcl2
Trem1
Nlrp3
Cxcl13
C1qa
Cd81
Hspa1b
C1qc
Ccl8
Hspa1a
H2-Eb1
Ccl5
C4b
H2-Aa
Vsig4
Cd74
Cd207
Cd163
H2-Ab1
Klf2
H2-K1
Folr2
Mrc1
Marco
H2-Q7
H2-D1
Klf4
Klf6
Cbr2
Mertk
D
Recruited
Resident
UMAP2
UMAP1
tdT Expression
0
>50
E
100
50
0
tdT Expression
Recruited
Resident

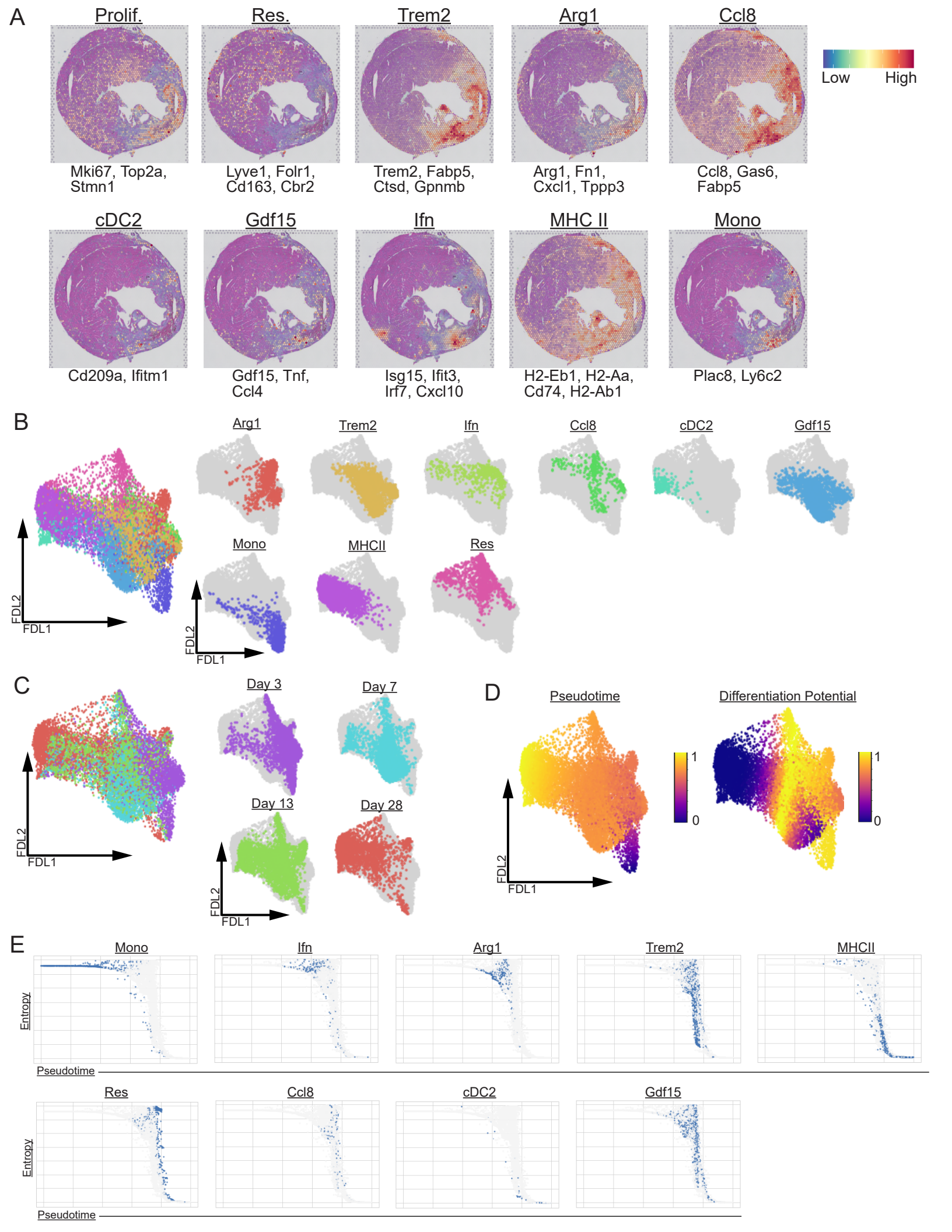
A
Prolif.
Mki67, Top2a, Stmn1
Res.
Lyve1, Folr1, Cd163, Cbr2
Trem2
Trem2, Fabp5, Ctsd, Gpnmb
Arg1
Arg1, Fn1, Cxcl1, Tppp3
Ccl8
Ccl8, Gas6, Fabp5
Low
High
cDC2
Cd209a, Ifitm1
Gdf15
Gdf15, Tnf, Ccl4
Ifn
Isg15, Ifit3, Irf7, Cxcl10
MHC II
H2-Eb1, H2-Aa, Cd74, H2-Ab1
Mono
Plac8, Ly6c2
B
Arg1
Trem2
Ifn
Ccl8
cDC2
Gdf15
Mono
MHCII
Res
FDL2
FDL1
C
Day 3
Day 7
Day 13
Day 28
D
Pseudotime
Differentiation Potential
1
0
E
Mono
Ifn
Arg1
Trem2
MHCII
Res
Ccl8
cDC2
Gdf15
Entropy
Pseudotime

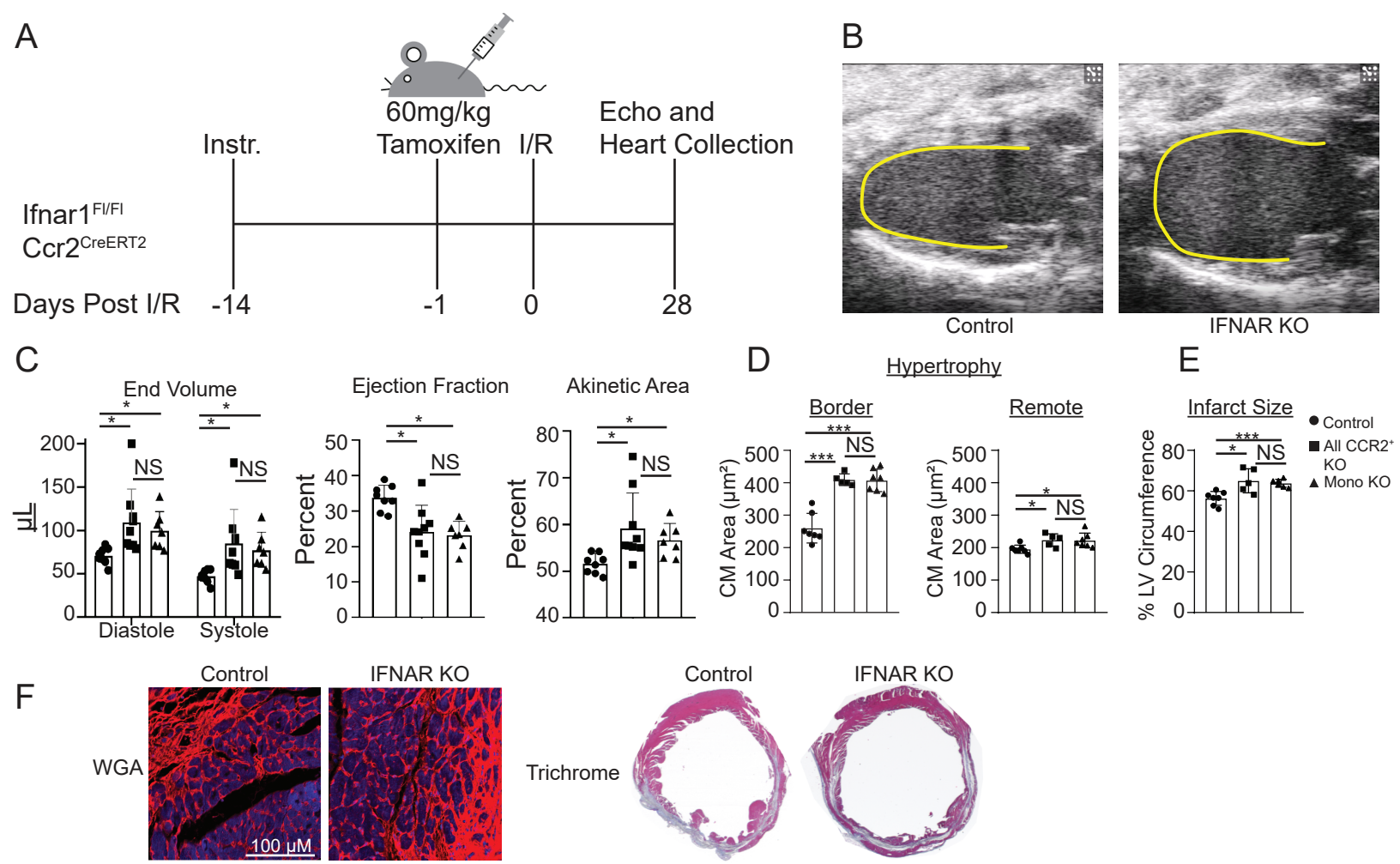
A
60mg/kg
Tamoxifen
Instr.
I/R
Echo and
Heart Collection
Ifnar1 Fl/Fl
Ccr2 CreERT2
Days Post I/R
-14
-1
0
28
B
Control
IFNAR KO
C
End Volume
Ejection Fraction
Akinetic Area
µL
Percent
Percent
NS
Diastole
Systole
D
Hypertrophy
Border
Remote
CM Area (µm²)
E
Infarct Size
% LV Circumference
Control
All CCR2+ KO
Mono KO
F
Control
IFNAR KO
WGA
100 µM
Trichrome